Control of a Single-Phase Cascaded H-Bridge Active Rectifier Under Unbalanced Load

Vojtech Blahnik, *Member, IEEE*, Tomas Kosan, Zdeněk Peroutka, *Member, IEEE*, and Jakub Talla

***Abstract*—Cascaded H-bridge (CHB) converter technology is actually the most popular solution for grid-connected converters in both medium- and high-voltage applications. This paper introduces a new control of a single-phase CHB active rectifier. The control uses a direct grid current control based on adaptive resonant controllers. The resonant controllers are adapting to slow fluctuation of ac grid frequency. The challenging problem of CHB converters is dc-link capacitor voltage balancing especially under unbalanced load conditions. This paper presents a reliable voltage-balancing technique utilizing energy estimation of particular dc-link capacitor banks and simple prediction of the changes of their energies. A nonlinear behavior of the converter caused by power semiconductors voltage drops and dead-time effects is minimized by auxiliary adaptive resonant controllers. The resulting control has very good performance, including the operation under unbalanced load conditions, and achieves low total harmonic distortion of converter grid current. The theoretical results were verified by experiments made on the developed CHB active rectifier prototype with three power cells in cascade.**

***Index Terms*—Current control, multilevel systems, rectifiers, regulators.**

I. Introduction

NOWADAYS, multilevel converters are used in a wide range of high-power applications including renewable energy resources, power transfer networks, high-power electric transport vehicles, etc. [1]. In the literature, there were published many multilevel topologies including neutral point clamped (NPC)/active NPC, flying capacitor, cascaded H-bridge (CHB) converters, and many other modifications [2]. This paper focuses on CHB converters, which are the most popular solution for grid-connected converters in both medium- and high-voltage applications at present (see, e.g., [2]–[5]). CHB converter technology is due to its power circuit simplicity, high flexibility, and adaptability favorite choice also in many other applications such as power electronics transformers [6], [7] or voltage-source inverters [8], [9]. Most of the existing applications are reported in three-phase systems. However, the CHB technology is very important also in single-phase systems. It represents promising technology for traction applications, specifically, for an input single-phase active rectifier for ac catenary supplied locomotives, electric multiple units (EMUs), and trainsets with medium-frequency transformers (MFTs). MFT-based converters resulting in significant weight savings of the vehicle have been one of the most important research objectives in traction in the last ten years [3], [7]. The next promising applications are active power filters and symmetrization units for traction substations [10].

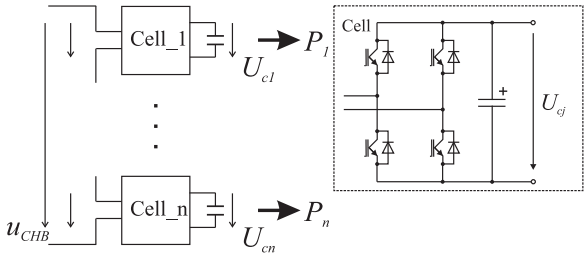

Fig. 1. N-level CHB converter topology.

A simplified power circuit of the CHB converter is shown in Fig. 1. The CHB converter consists of serial-connected power cells. Each cell contains an H-bridge converter with a separated dc-link capacitor. The higher number of cells increases the number of possible converter voltage levels. In addition, more converter voltage levels result in lower grid current ripple and, therefore, lower total harmonic distortion (THD) of the grid current [7]. On the other hand, the higher number of cascaded cells complicates the converter control, especially in the terms of circulating current control and balancing of the voltage on the particular dc links [11]. This paper investigates the control of a single-phase CHB active rectifier under unbalanced load conditions.

The control of active rectifiers typically consists of dc-side voltage control, grid current control, and grid voltage synchronization. Furthermore, the CHB multilevel rectifiers need an active balancing of dc-link voltages, especially when the dc-side load is unbalanced as mentioned above.

Very simple and robust methods based on hysteresis current control of active rectifiers are presented in [12]. These types of control preclude using of pulse width modulation (PWM). The main drawbacks of these methods are undetermined current spectra and variable switching frequency. The most commonly used PWM-based active and reactive power control methods

Manuscript received November 25, 2016; revised June 2, 2017; accepted August 19, 2017. Date of publication August 31, 2017; date of current version February 22, 2018. This work was supported by the Ministry of Education, Youth, and Sports of the Czech Republic under the RICE—New Technologies and Concepts for Smart Industrial Systems (Project LO1607). Recommended for publication by Associate Editor T. Shimizu. *(Corresponding author: Vojtech Blahnik.)*

The authors are with the Regional Innovation Centre for Electrical Engineering, Faculty of Electrical Engineering, University of West Bohemia, 301 00 Pilsen, Czech Republic (e-mail: lucke@kev.zcu.cz; kosan@rice.zcu.cz; peroutka@ieee.org; talic@rice.zcu.cz).

Color versions of one or more of the figures in this paper are available online at http://ieeexplore.ieee.org.

Digital Object Identifier 10.1109/TPEL.2017.2748218

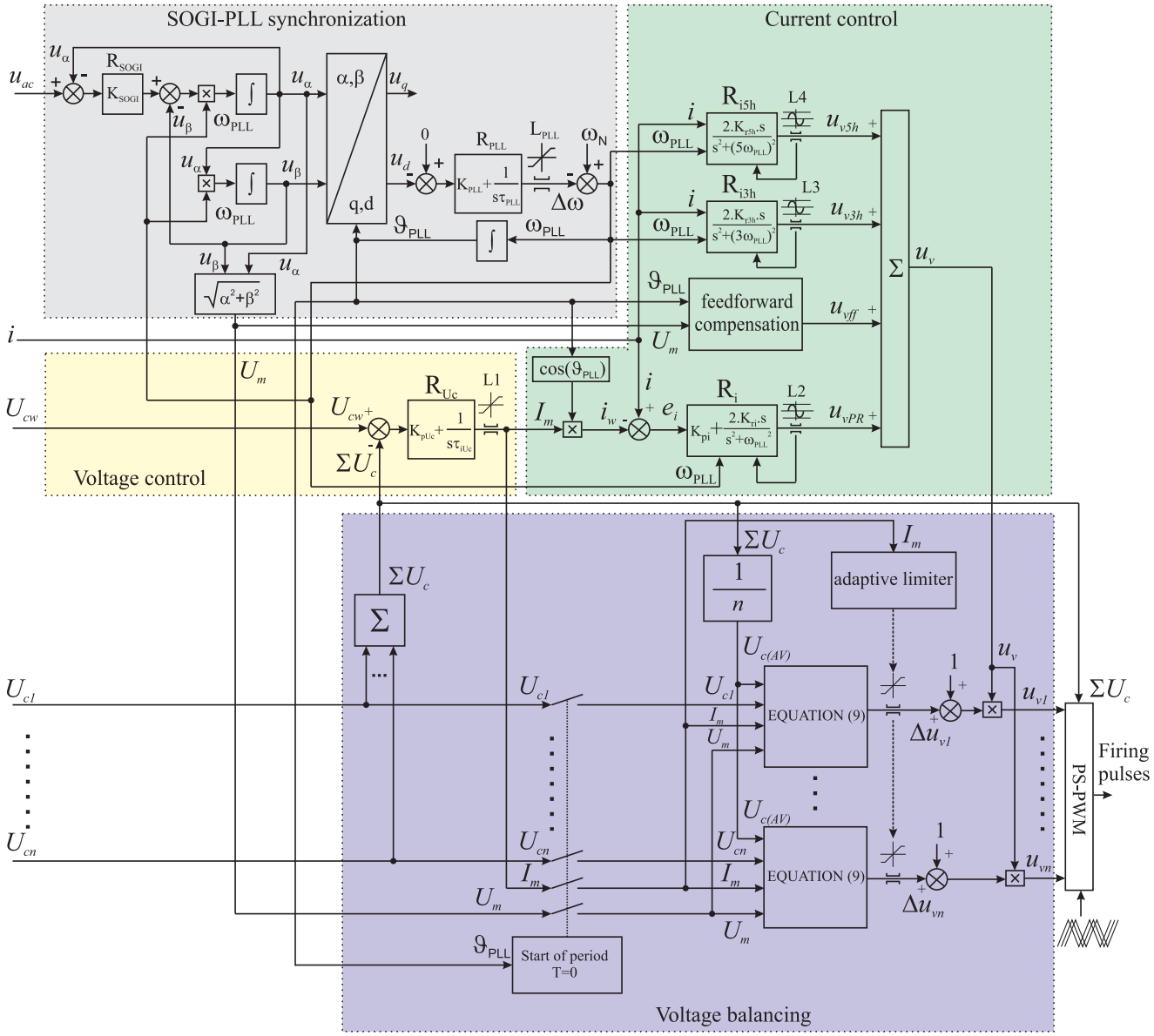

Fig. 2. Proposed single-phase CHB active rectifier control.

utilize vector control theory (dq and PQ control) [13], [14]. Recently investigated control methods are based on model-predictive control [11], [15]. These types of controllers are sensitive to the system model accuracy and typically computationally expensive.

Control of single-phase active rectifiers is a special problem [16]. For single-phase systems, the vector control methods have limited advantages over stationary reference frame methods due to difficulties with transformation to a rotating reference frame. The instantaneous values of voltage and current of single phase are measured only. Thus, it is not possible to transform these values to the dq rotating system directly. Therefore, the stationary reference frame control based on proportional–resonant (PR) controllers is very popular [17], [18]. PR controllers are capable to track sinusoidal current references of required frequencies of both positive and negative sequences with zero steady-state error. The resonant controller works well when the frequency of the controlled signal is fixed. However, the grid frequency varies. Therefore, we propose in this paper an adaptation algorithm of the resonant controllers used in the converter control (see Section II-B). The controller adaptation requires the information about the actual grid frequency, which is estimated by the grid synchronization algorithm.

A synchronization of the control with the grid voltage is very important part of active rectifier control, because the grid current is controlled with respect to the grid voltage phase. The most popular methods for synchronization in single-phase systems are based either on discrete Fourier transform (DFT) or on phase-locked-loop (PLL) methods. DFT methods are robust and resistant to noise and disturbances. On the other hand, PLL-based methods can respect the grid frequency fluctuation. Accurate synchronization of the control with the grid in single-phase

systems is not easy to achieve. A typical PLL synchronization in three-phase systems use Clarke and Park transform. The Clarke transform is not usable in single-phase systems. The most common methods to obtain real and imaginary parts of the signal in single-phase systems are differentiation [19], quarter cycle delay [20], or second-order generalized integrator (SOGI) [21]. The SOGI-PLL uses the second-order general integration part to substitute the Clarke transform. The main advantage over previously mentioned methods is much higher robustness to disturbances. The properly tuned SOGI-PLL provides enough robust and fast synchronization in most of the power grids. The SOGI-PLL method [22] was selected for grid voltage synchronization in our case (see more details in Section II-A).

Different methods for balancing dc-link voltage capacitors have been published [23]–[26]. The model-predictive current control of CHB converters [23], [24] demonstrated good controller performance in terms of grid current waveform quality and power factor correction. The drawback of the presented method is control under unbalanced loads. It does not provide a proper control function when the loads of particular H-bridge cells are different. Commonly applied algorithms for voltage cell balancing use a proportional–integral (PI) controller [27], [28]. The other popular balancing methods operate directly at modulation level [26], [29]. However, these methods do not provide precise current control. In [25], passivity-based control designed via energy consideration for an N-level H-bridge active rectifier is introduced. This interesting approach provides full decoupling of the H-bridges and separate control of each cell. This paper presents the energy estimation algorithm with dc-link capacitor balancing based on predicted (calculated) change of particular dc-link energy. This approach is explained in Section II-B1.

II. Converter Control

This section describes the proposed control of a single-phase CHB active rectifier. The control is composed of synchronization with the grid voltage, direct grid current control, output dc-link voltage control, and voltage-balancing algorithm, as shown in Fig. 2.

A. SOGI-PLL Grid Voltage Synchronization

A synchronization with the single-phase grid voltage must provide fast and correct estimation of actual grid voltage vector u_{ac} (voltage vector amplitude U_m, voltage vector position ϑ_{PLL}, and grid frequency ω_{PLL}). The SOGI-PLL synchronization method is easy to implement with fast response behavior and with sufficient immunity to disturbances of input signal. This synchronization technique is known, e.g., from [22] and [30], where it is used for both single-phase and three-phase systems. The block diagram of the proposed SOGI-PLL synchronization and its cooperation with remaining part of the proposed control is shown in Fig. 2.

The SOGI-PLL consists of two basic parts. The first part is the SOGI part, which estimates the real (u_α) and imaginary (u_β) parts of the input signal (u_{ac}) in the stationary reference frame. The SOGI open-loop transfer function is derived in the Laplace transform in (1), where s represents a Laplace operator.

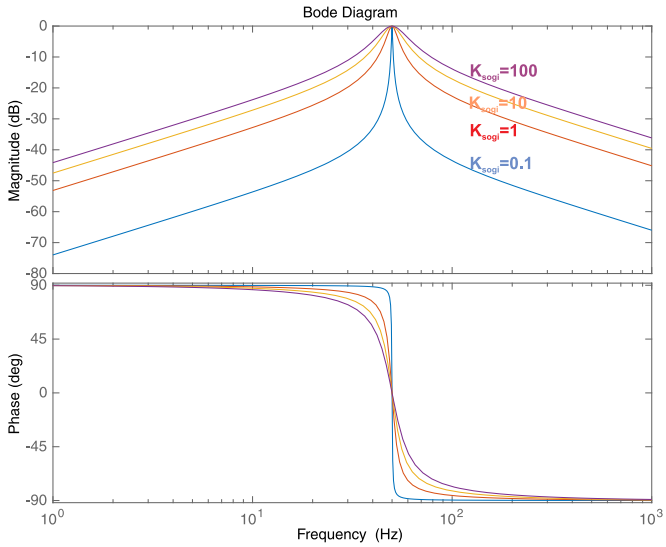

Fig. 3. SOGI part closed-loop Bode characteristic.

Substituting (2) into (1), we obtain an SOGI transfer function (3), which has exactly the same form as a resonant controller. Thus, the SOGI part can be interpreted as a combination of the resonant controller in the feedforward path and the negative feedback signal formed by resonant controller output (u_α). The SOGI response to input signal (u_{ac}) depends on the closed-loop transfer function, which is described by (4). From (4), it is evident that the SOGI dynamics and stability is influenced only by K_{SOGI} . The K_{SOGI} must be set as a compromise between the quality of the input signal and requirements on the speed of the SOGI response, as explained in Fig. 3. If the K_{SOGI} is high, the Bode characteristic of the SOGI closed loop has a wide bandwidth and allows the fast transient response (see Fig. 3). On the other hand, the noise and voltage disturbances could transmit through the SOGI part less attenuated. Typically, disturbance rejection is preferred, and therefore, K_{SOGI} is selected to be lower. In our case, K_{SOGI} was set to 0.1

$$F_{\mathrm{SOGI_{OL}}} = \frac{U_\alpha(s)}{U_{\mathrm{ac}}(s) - U_\alpha(s)} = K_{\mathrm{SOGI}} \frac{s\,\omega_{\mathrm{PLL}}}{s^2 + {\omega_{\mathrm{PLL}}}^2} \tag{1}$$

$$K_{r_{\mathrm{SOGI}}} = \frac{K_{\mathrm{SOGI}}\omega_{\mathrm{PLL}}}{2} \tag{2}$$

$$F_{\mathrm{SOGI_{OL}}} = \frac{2\,K_{r_{\mathrm{SOGI}}} s}{s^2 + {\omega_{\mathrm{PLL}}}^2} \tag{3}$$

$$F_{\mathrm{SOGI_{CL}}} = \frac{U_\alpha(s)}{U_{\mathrm{ac}}(s)} = \frac{F_{\mathrm{SOGI_{OL}}}}{1 + F_{\mathrm{SOGI_{OL}}}}. \tag{4}$$

The second part of the SOGI-PLL is the PLL part. It consists of the stationary reference frame to rotating reference frame transform ($\alpha\beta/dq$) and PI controller influencing the speed of the PLL locking. The PI controller regulates a reactive component of the grid voltage (u_d) to zero. The PI controller output signal (correction signal $\Delta\omega$) changes the angular velocity of the virtual rotating reference frame relatively to the grid nominal frequency ω_N. The high proportional gain leads to wider bandwidth of the closed loop but with the drawback of low

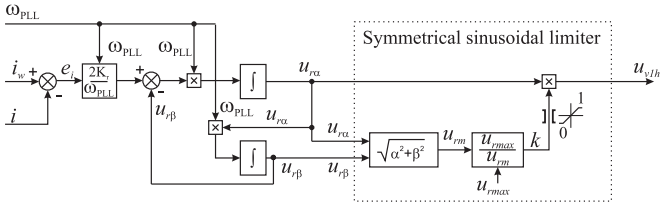

Fig. 4. Detail block diagram of the proposed adaptive resonant controller.

disturbance attenuation. The short time constant causes the faster transient response with the drawback of higher transient overshoot [31]. In general, the PI controller coefficient setting for voltage synchronization in conventional grids does not require high dynamic frequency response due to low speed of grid frequency fluctuation. The expected maximum grid frequency deviation is in the range from 48 to 52 Hz with the maximum rate of its change of 1 Hz $\cdot$ s^{-1}. In our case, the PI saturation limiter is set to ± 3 Hz, $K_{\mathrm{PLL}} = 0.1$, and $\tau_{\mathrm{PLL}} = 0.5$ s. To speed up SOGI-PLL lock out, a simple startup condition was proposed—SOGI-PLL input signal u_{ac} is blocked until grid voltage reaches its amplitude, i.e., derivation of grid voltage is close to zero.

B. DC-Link Voltage and Grid Current Control

The total output dc-link voltage computed as a sum of dc-link voltages of all particular cells is controlled to required value U_{cw} by the PI regulator R_{Uc}. The regulator (R_{Uc}) commands the magnitude of the required grid current I_m. The actual value of reference current i_w is calculated by (5) and compared with the measured grid current i. The resulting error signal e_i enters into the adaptive PR controller R_i. The controller generates signal u_{vPR}, which is summed in the following step with a feedforward term u_{vff} calculated by a feedforward compensation block described in detail below. For compensation of harmonics disturbances caused by dead-time effects and nonlinear voltage drops on power electronics switches, the current control is supplemented by additional adaptive resonant controllers for third and fifth harmonic elimination. Advantages of this solution for the single-phase H-bridge rectifier were described, e.g., in [32]

$$i_w = I_m \cos(\vartheta_{\mathrm{PLL}}). \tag{5}$$

1) Adaptive Grid Current PR Controller: The PR grid current controller R_i consists of proportional (P) and adaptive resonant (R) controllers. The ordinary type of the R controller is a preferred solution for direct current control [33], [34] in single-phase systems. The main disadvantage of the R controller is current phase shift generated by different controller frequencies against actual grid frequency. The magnitude Bode plot of the R controller has a very sharp shape. The common resonant controller considers fixed frequency. However, the fundamental grid frequency is variable. A grid frequency can fluctuate up to ± 2 Hz. For this reason, the output signal of the SOGI-PLL (ω_{PLL}) is used for the R controller adaptation. The block diagram of an improved R controller is introduced in Fig. 4. The R controller frequency is not fixed, but it depends on the real grid frequency

$$F_r = \frac{2K_r}{\omega_{\mathrm{PLL}}} \frac{\omega_{\mathrm{PLL}}\, s}{s^2 + {\omega_{\mathrm{PLL}}}^2} = \frac{2K_r s}{s^2 + {\omega_{\mathrm{PLL}}}^2}. \tag{6}$$

This allows precise grid current control during grid frequency fluctuations. The R controller is further improved by a symmetrical sinusoidal limiter. The controller output signal $u_{r\alpha}$ is delayed by integral block to $u_{r\beta}$ (imaginary part of virtual vector composed of components $u_{r\alpha}$ and $u_{r\beta}$). The amplitude u_{rm} of the created virtual vector is calculated from its components $u_{r\alpha}$ and $u_{r\beta}$. If u_{rm} is higher than $u_{r\max}$ (set value of limiter), then $u_{r\alpha}$ is limited by factor $k = (u_{r\max}/u_{rm})$ according to Fig. 4. Thus, the amplitude of output signal u_{vx} of the resonant controller is limited to $u_{r\max}$. The value of $u_{r\max}$ is defined by (7), where $\xi \in (0, 1)$ is a safety coefficient. Typically, $\xi = 0.9$

$$u_{r\max} = \xi \sum_{j=1}^{n} U_{cj}. \tag{7}$$

2) Feedforward Compensation: The direct grid current control based on the above-described adaptive PR controller is supplemented by a feedforward compensation block composed of (8) and (9)

$$\varepsilon = \arctan \frac{\omega_N L I_m}{U_m} \tag{8}$$

$$u_{\mathrm{vff}} = \frac{U_m}{\cos(\varepsilon)} \sin(\vartheta_{\mathrm{PLL}} - \varepsilon) \tag{9}$$

where I_m is the amplitude of the required grid current, ω_N is the nominal grid frequency, L is the inductance of a filter at the converter ac side, U_m is the amplitude of the grid voltage, ϑ_{PLL} is the position of the grid voltage vector, and ε presents the displacement of the feedforward voltage vector versus the grid voltage vector. The feedforward term u_{vff} is calculated according to (9).

3) Low-Frequency Harmonics Compensator: The low-frequency harmonics are compensated by a bank of the proposed adaptive resonant controllers with frequency tracking and output limiter, as described in Fig. 4. In this case, we demonstrate an elimination of third and fifth harmonics (150 and 250 Hz). More information about low-frequency harmonic compensation by resonant controllers can also be found, e.g., in [32] and [34].

C. Voltage Balancing

The voltage-balancing block secures (see Fig. 2) balancing of voltages on separated dc-link capacitors of cascaded power cells. Input signals are dc-link voltages in the case of generally n cascaded cells denoted U_{c1}, U_{c2}, ..., U_{cn} (see Fig. 1), amplitude of required grid current I_m, grid voltage vector amplitude U_m, grid voltage vector position ϑ_{PLL}, and virtual modulation signal for the complete CHB converter u_v (u_v is the output of the converter control before application of the balancing algorithm). The resulting control signals for particular CHB cells are u_{v1}, u_{v2}, ..., u_{vn}. These control signals are used as a modulation signals for phase-shifted PWM (PS-PWM). The corrections of modulation signal $\Delta u_{v1\%}$, $\Delta u_{v2\%}$, ..., $\Delta u_{vn\%}$ for each separated power cell are calculated once per period of the grid voltage (T). The

correction signal is determined from average dc-link voltage $U_{c(AV)}$, from the dc-link voltage at the given power cells U_{cj} where $j = 1, 2, ..., n$, from the estimated grid voltage amplitude U_m, and from the demanded grid current amplitude I_m.

The proposed energy-balancing method is based on the balance between the energies ΔW_{cj} and ΔW_{ARj}. The energy ΔW_{cj} given by (10) is required to charge the dc link of the jth cell to $U_{c(AV)}$, ΔW_{ARj} given by (11) is the energy which the grid is able to deliver in one period of the grid voltage to the jth cell. From the equality of these energies (12), it is possible to express by (13) required grid current correction ΔI_{mj}. The correction of the modulation signal for the given power cell $\Delta u_{vj\%}$ is calculated from (14). The balancing method behaves as a proportional controller of capacitor energies with adaptive gain scheduling. The exact proportional gain is calculated to minimize the energies errors during one period of the grid voltage. The main advantage is high-voltage-balancing dynamics and robustness. On the other hand, all variances in system parameters and measurements errors lead to a small steady-state error.

An important part of the balancing algorithm is an adaptive limiter influencing the correction signal $\Delta u_{vj\%}$ considering demanded grid current amplitude I_m. The limiter implements the deadband of balancing signals according to the demanded grid current I_m. For I_m in the range of $\pm 5\%$ of nominal I_m, the correction signals $\Delta u_{v1\%}$, $\Delta u_{v2\%}$, ..., $\Delta u_{vn\%}$ are set to zero. Thus, the limitation directly depends on actual converter power. The resulting modulation signal u_{vj} for the given power cell is calculated by (15)

$$\Delta W_{cj} = \frac{1}{2} C \left(U_{c(AV)}^2 - U_{cj}^2 \right) \tag{10}$$

$$\Delta W_{ARj} = \frac{1}{n} \frac{U_m}{\sqrt{2}} \frac{\Delta I_m}{\sqrt{2}} = \frac{1}{n} \frac{U_m \Delta I_{mj}}{2} T \tag{11}$$

$$\frac{1}{2} C \left(U_{c(AV)}^2 - U_{cj}^2 \right) = \frac{1}{n} \frac{U_m \Delta I_{mj}}{2} T \tag{12}$$

$$\Delta I_{mj} = \frac{nC(U_{c(AV)}^2 - U_{cj}^2)}{U_m T} \tag{13}$$

$$\Delta u_{vj\%} = \frac{\Delta I_{mj}}{I_m} = \frac{nC(U_{c(AV)}^2 - U_{cj}^2)}{U_m T I_m} \tag{14}$$

$$u_{vj} = (\Delta u_{vj\%} + 1) u_v. \tag{15}$$

Under the fault condition in one cell (H-bridge), it is necessary to bypass the faulty cell and change parameters in the balancing algorithm. The parameter n has to be changed to actual number of active cells. Blocking voltage of the remaining cells has to withstand a new higher dc link voltage or the total voltage must be reduced.

III. Developed Laboratory Prototype

A power circuit of the developed laboratory prototype of a single-phase CHB active rectifier is shown in Fig. 5. Its parameters are listed in Table I. The programmable power source by AMETEK CSW 5550 has been used as an intelligent grid emulator ($u_{\rm ac}$). The common inductor of 4 mH is used as an input filter L with a parasitic resistance R of 0.15 Ω. The seven-level CHB (7L-CHB) converter is composed of three separate H-bridge converters. In this case, each cell load is realized separately by the single H-bridge inverter with a resistor connected on its ac side. This solution allows us to set load of each rectifier cell independently to other ones. The testing converter topology in Fig. 5 has been motivated by our research of ac catenary supplied suburban units (EMUs) with an MFT, which is the target application for the technology presented in this paper.

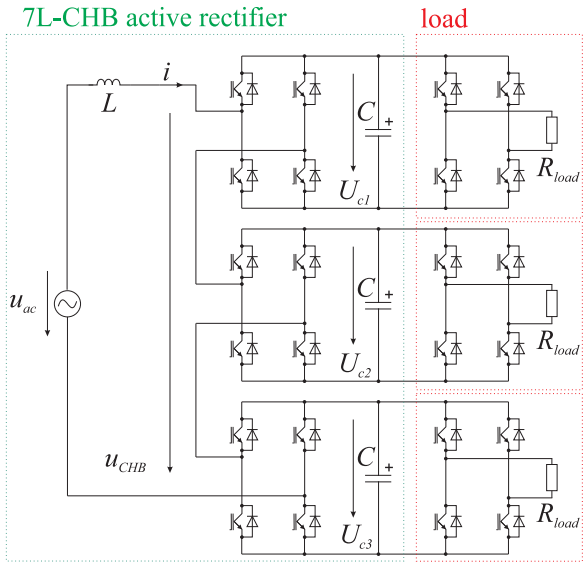

Fig. 5. Power circuit of the developed CHB active rectifier laboratory prototype.

TABLE I
Parameters of the Laboratory Prototype

Symbol	Title	Value
$u_{\rm ac}$	Rated grid voltage	230 V_{RMS}
f_N	Rated grid frequency	50 Hz
L	Input filter inductor	4 mH
C	DC-link capacitor of each HB cell	3.4 mF
U_{cw}	Required total dc-link voltage	450 V
$U_{c1} = U_{c2} = U_{c3}$	Nominal voltage for each cell	150 V
$f_{\rm pwm}$	Switching frequency of IGBTs	1 kHz
	Deadtime	3 μs

The insulated-gate bipolar transistor (IGBT) modules SKM195GB126D are used for the laboratory prototype of the converter. The switching frequency of IGBTs is fixed to 1 kHz. However, the resulting frequency of current ripple is 6 kHz. This is caused by using of PS-PWM and zero-vector alternating modulation technique. A detail description of the modulator used for the 7L-CHB converter can be found in [35].

The proposed control of the CHB active rectifier has been implemented in the floating-point digital signal processor Texas Instruments TMS320F28335. The output modulation signals (u_{v1}, u_{v2}, and u_{v3}) are used for the PS-PWM-based modulator implemented in the field-programmable gate array Altera EP3C40. Both devices are placed on the development control

TABLE II
CONTROL SYSTEM SETTING

Regulator	Type	Parameter	Value	Unit
R_{Uc}	PI	K_{pUc}	0.1	[-]
		τ_{iUc}	0.2	[s]
R_i	PR	K_{pi}	2.0	[-]
		K_{ri}	100.0	[-]
$\mathrm{R_{i3h}}$	R	K_{r3h}	50.0	[-]
$\mathrm{R_{i5h}}$	R	K_{r5h}	10.0	[-]

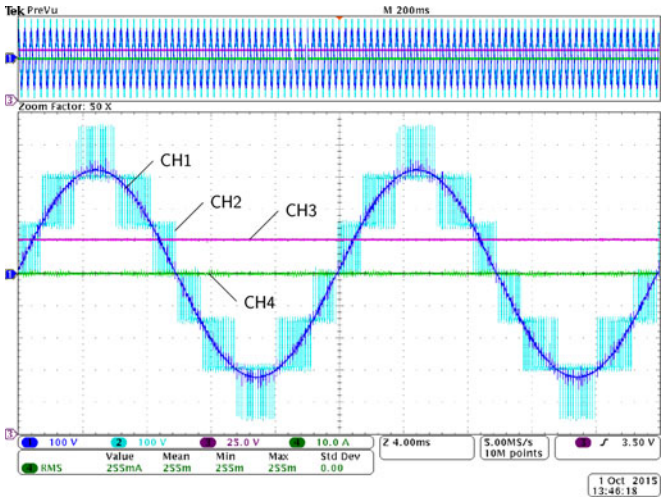

Fig. 6. CHB active rectifier under steady-state conditions (no-load). CH1: grid voltage u_{ac} [100 V/div], CH2: voltage on CHB ac terminals u_{CHB} [100 V/div], CH3: dc-link voltage of first HB U_{c1} [25 V/div], CH4: grid current i [10 A/div].

board designed for control of multilevel converters; for more details, see [36]. The setting of the controllers is provided in Table II.

IV. EXPERIMENTAL RESULTS

The employed PS-PWM ensures the small grid current ripple, which is a consequence of phase-shifted modulation for each H-bridge cell. The converter behavior under steady-state conditions is analyzed in Fig. 6 (converter without load) and in Fig. 7. (converter loaded by 4 kW, symmetrical load). In this particular case, the 7L-CHB active rectifier with switching frequency of 1 kHz has grid current ripple frequency around 6 kHz. The result of harmonic analysis of the grid current (i) during symmetrical load of 4 kW is shown in Fig. 8. The resulting grid current THD_i reaches 1.05% only. The THD_i was calculated up to the $50\mathrm{th}$ harmonics (2500 Hz) according to (16) given in [37]

$$\mathrm{THD}_i = \sqrt{\sum_{h=2}^{50}\left(\frac{I_h}{I_1}\right)}. \tag{16}$$

The active rectifier response to the step change of the load from 0 to 4 kW (symmetrical loaded) is documented in Fig. 9. The proper function of the proposed voltage-balancing block is reported in Figs. 10–13. During these tests, the CHB rectifier was loaded by unbalanced load (second HB is loaded by 80% load

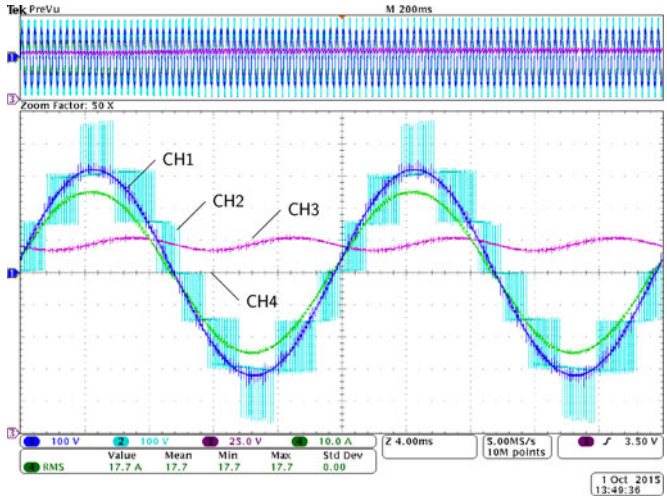

Fig. 7. CHB active rectifier under steady-state conditions (symmetrical load of 4 kW). CH1: grid voltage u_{ac} [100 V/div], CH2: voltage on CHB ac terminals u_{CHB} [100 V/div], CH3: dc-link voltage of first HB U_{c1} [25 V/div], CH4: grid current i [10 A/div].

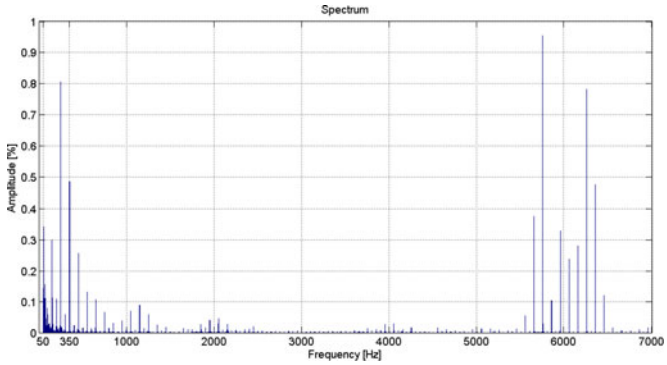

Fig. 8. Grid current harmonic analysis of the CHB active rectifier under symmetrical load of 4 kW, $\mathrm{THD}_i = 1.05\%$.

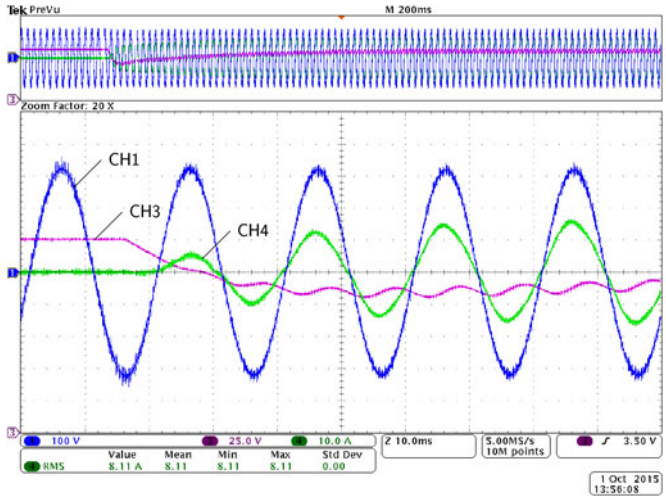

Fig. 9. CHB active rectifier under step change of load from 0 to 4 kW (symmetrical load). CH1: grid voltage u_{ac} [100 V/div], CH3: dc-link voltage first HB U_{c1} [25 V/div], CH4: grid current i [10 A/div].

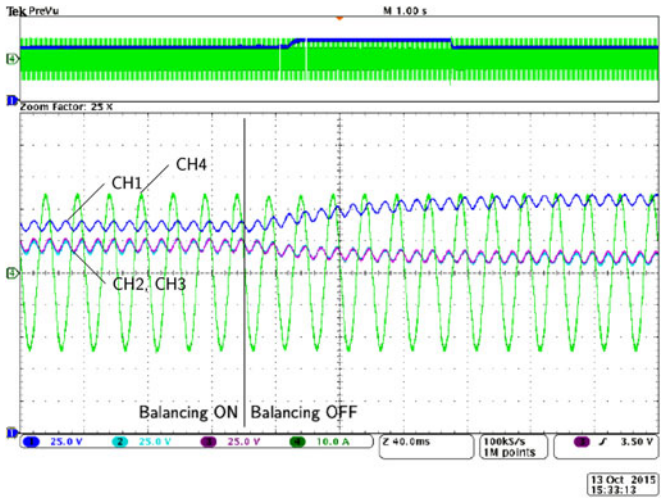

Fig. 10. CHB active rectifier under unbalanced load after balancing switched-off (second HB loaded 80%, load of 4 kW). CH1: dc-link voltage second HB U_{c2} [25 V/div], CH2: dc-link voltage third HB U_{c3} [25 V/div], CH3: dc-voltage first HB U_{c1} [25 V/div], CH4: grid current i [10 A/div].

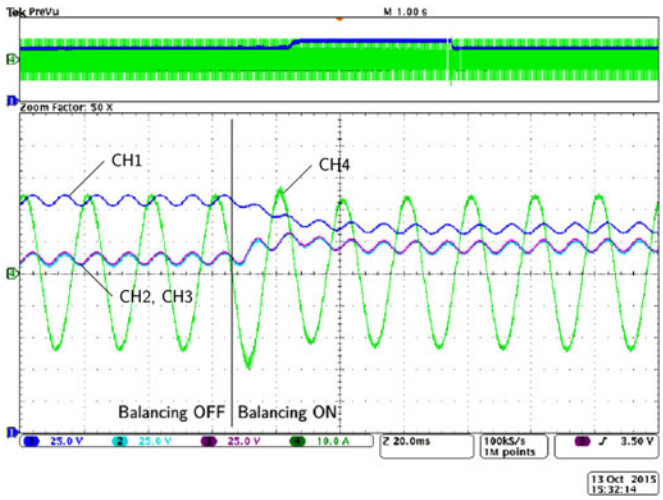

Fig. 11. CHB active rectifier under unbalanced load after balancing switched-on (second HB loaded 80%, load of 4 kW). CH1: dc-link voltage second HB U_{c2} [25 V/div], CH2: dc-link voltage third HB U_{c3} [25 V/div], CH3: dc-voltage first HB U_{c1} [25 V/div], CH4: grid current i [10 A/div].

against first and third). Fig. 10 presents converter behavior after switching OFF the voltage-balancing block. Fig. 11 displays the converter behavior after switching the voltage-balancing block ON. When the proposed voltage-balancing strategy is in operation, the difference between the dc-link voltages of particular power cells is significantly reduced even if their loads are extremely different. The dc-link voltages of all H-bridge cells have not exactly the same voltage as has been described in Section II-B1, but the presented steady-state error is acceptable. The steady-state converter behavior under unbalanced load (second HB is loaded by 80% load against first and third) is analyzed in Fig. 12, and the respective harmonic analysis is provided in Fig. 13. In this case, the grid current i has bigger ripple in comparison with the experiment shown in Fig. 7 (symmetrical

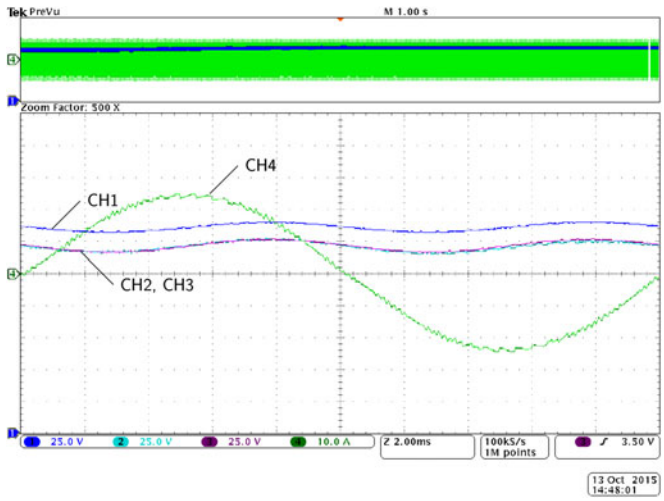

Fig. 12. CHB active rectifier under unbalanced load (second HB loaded 80%, load of 4 kW). CH1: dc-link voltage second HB U_{c2} [25 V/div], CH2: dc-link voltage third HB U_{c3} [25 V/div], CH3: dc-voltage first HB U_{c1} [25 V/div], CH4: grid current i [10 A/div].

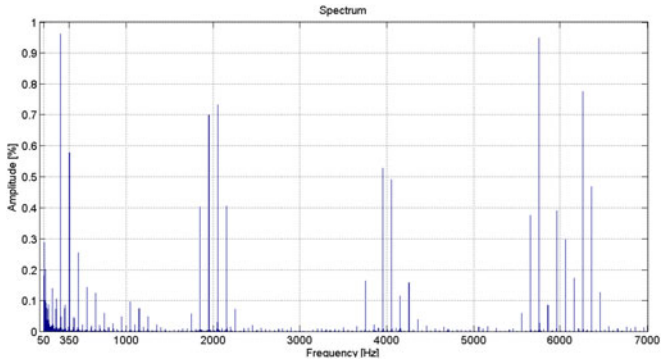

Fig. 13. Grid current harmonic analysis of the CHB active rectifier under the load of 4 kW (unbalanced load second HB loaded 80%, load of 4 kW), $\text{THD}_i = 1.71\%$.

TABLE III
CURRENT THD_i FOR SYMMETRICAL AND UNBALANCED LOADS

Second HB load	Type of load	THD_i
100%	Symmetrical load 4 kW	1.05%
90%	Unbalanced load 4 kW	1.34%
80%	Unbalanced load 4 kW	1.71%
70%	Unbalanced load 4 kW	2.11%
60%	Unbalanced load 4 kW	2.7%
50%	Unbalanced load 4 kW	3.34%

load). This fact is caused by different control signals of each HB cell. For this reason, there is also an important difference in the harmonic analysis results. The current interferences appeared at frequencies lower than 2500 Hz, and the resulting THD_i thus increased to 1.71% (monitored according to [37]). Table III shows the dependence of grid current THD_i on unbalanced load of the CHB active rectifier. In these experiments, the first and third HBs had the same load, while the second HB had a different

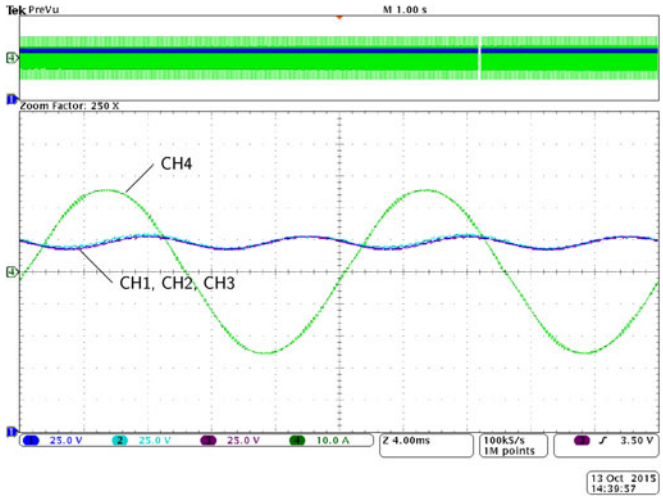

Fig. 14. CHB active rectifier under symmetrical load with reduced second HB dc-link capacitance to 2.5 mF, load of 4 kW. CH1: dc-link voltage second HB U_{c2} [25 V/div], CH2: dc-link voltage third HB U_{c3} [25 V/div], CH3: dc-voltage first HB U_{c1} [25 V/div], CH4: grid current i [10 A/div].

load mentioned in the first column of the table. Under balanced load, the grid current ripple frequency is of 6 kHz in the case of switching frequency of 1 kHz. However, modulation signals are significantly modified for particular cells under unbalanced load conditions. Therefore, the unbalanced load excites undesirable interferences in the grid current. The current interferences appeared at frequencies below 2.5 kHz (dominant frequencies are 2, 4, and 6 kHz). This is the main reason for increasing of THD_i, which is calculated according to (16). The highest THD_i was achieved below 5% (exactly 3.34% under 50% unbalance in the load; see Table III), which is in most of the applications an acceptable result. Analysis of PS-PWM harmonic distortion is in detail described, e.g., in [38]. Fig. 14 shows performance of the balancing algorithm under unequal dc-link capacitors in particular power cells. The dc-link capacitance of the second cell was lowered to 2.5 mF from original 3.4 mF.

V. Conclusion

This paper presents new simple and computationally effective control algorithm for single-phase CHB active rectifiers. The proposed control algorithm is resistant to grid parameter variations and unbalanced load conditions. Due to the adaptation of current controllers, the rectifier can reliably operate in grids with expected significant fluctuations of grid voltage amplitude and frequency.

The grid current control consists of PR controller extended by auxiliary resonant (R) controllers for grid current THD_i reduction and feedforward term calculation. The R controllers were improved by grid frequency adaptation and an output limiter based on the actual dc-link voltage. The main and auxiliary resonant controllers are adapted to variable fundamental grid frequency to avoid current phase shift. The sinusoidal limiter prevents grid current distortion caused by insufficient dc-link voltage. In addition, the actual grid voltage amplitude and phase, estimated by the SOGI-PLL, is used in feedforward term calculation to improve current control dynamics.

The proposed voltage control consists of the main PI dc-link voltage controller and voltage-balancing algorithm based on energy estimation. The balancing algorithm calculates energy of particular dc-link capacitor banks and simply predicts changes of their energies. The balancing method performs fine under balanced strongly unbalanced load conditions as well as under unequal dc-link capacitors in particular power cells. However, it is not possible to balance dc-link voltages of all power cells to the same value exactly. There is still small, but nonzero, steady-state control error, because the voltage balancing is implemented as a feedforward calculation. On the other hand, simplicity, robustness, and high dynamic voltage balancing without any voltage overshoots are the main advantages of this method.

The presented control of the CHB active rectifier was successfully tested using the developed converter prototype under both symmetrical and unbalanced load conditions. Spectral analyses of the grid current under unbalanced load conditions showed expected rise of low-frequency harmonics and THD_i. The control of the single-phase CHB active rectifier has been able to satisfy all the commands with very good dynamics, and the expected voltage-balancing errors have been acceptable and in compliance with defined converter design parameters.

References

[1] L. G. Franquelo, J. Rodriguez, J. I. Leon, S. Kouro, R. Portillo, and M. A. M. Prats, "The age of multilevel converters arrives," *IEEE Ind. Electron. Mag.*, vol. 2, no. 2, pp. 28–39, Jun. 2008.

[2] S. Kouro *et al.*, "Recent advances and industrial applications of multilevel converters," *IEEE Trans. Ind. Electron.*, vol. 57, no. 8, pp. 2553–2580, Aug. 2010. [Online]. Available: http://dblp.uni-trier.de/db/journals/tie/tie57.html#KouroMGPFWRPG10

[3] M. Steiner and H. Reinold, "Medium frequency topology in railway applications," in *Proc. Eur. Conf. Power Electron. Appl.*, Sep. 2007, pp. 1–10.

[4] G. P. Adam, I. A. Abdelsalam, K. H. Ahmed, and B. W. Williams, "Hybrid multilevel converter with cascaded H-bridge cells for HVDC Applications: Operating principle and scalability," *IEEE Trans. Power Electron.*, vol. 30, no. 1, pp. 65–77, Jan. 2015.

[5] Y. Neyshabouri, H. Iman-Eini, and M. Miranbeigi, "State feedback control strategy and voltage balancing scheme for a transformer-less STATic synchronous COMpensator based on cascaded H-bridge converter," *IET Power Electron.*, vol. 8, no. 6, pp. 906–917, 2015.

[6] M. Vasiladiotis and A. Rufer, "A modular multiport power electronic transformer with integrated split battery energy storage for versatile ultrafast EV charging stations," *IEEE Trans. Ind. Electron.*, vol. 62, no. 5, pp. 3213–3222, May 2015.

[7] C. Zhao *et al.*, "Power electronic traction transformer medium voltage prototype," *IEEE Trans. Ind. Electron.*, vol. 61, no. 7, pp. 3257–3268, Jul. 2014.

[8] M. Coppola, F. D. Napoli, P. Guerriero, D. Iannuzzi, S. Daliento, and A. D. Pizzo, "An FPGA-based advanced control strategy of a gridTied PV CHB inverter," *IEEE Trans. Power Electron.*, vol. 31, no. 1, pp. 806–816, Jan. 2016.

[9] A. J. Watson, P. W. Wheeler, and J. C. Clare, "A complete harmonic elimination approach to DC link voltage balancing for a cascaded multilevel rectifier," *IEEE Trans. Ind. Electron.*, vol. 54, no. 6, pp. 2946–2953, Dec. 2007.

[10] X. Zhu, M. Chen, S. Xie, and J. Luo, "Research on new traction power system using power flow controller and Vx connection transformer," in *Proc. IEEE Int. Conf. Intell. Rail Transp.*, Aug. 2016, pp. 111–115.

[11] A. M. Lopez, D. E. Quevedo, R. Aguilera, T. Geyer, and N. Oikonomou, "Validation of a reduced order model for modular multilevel converters and analysis of circulating current," in *Proc. 17th Eur. Conf. Power Electron. Appl.*, Sep. 2015, pp. 1–10.

[12] M. Khazraei, H. Sepahvand, M. Ferdowsi, and K. A. Corzine, "Hysteresis-based control of a single-phase multilevel flying capacitor active rectifier," *IEEE Trans. Power Electron.*, vol. 28, no. 1, pp. 154–164, Jan. 2013.
[13] V. Valouch, M. Bejvl, P. Imek, and J. kramlk, "Power control of grid-connected converters under unbalanced voltage conditions," *IEEE Trans. Ind. Electron.*, vol. 62, no. 7, pp. 4241–4248, Jul. 2015.
[14] E. Behrouzian, M. Bongiorno, and R. Teodorescu, "Impact of switching harmonics on capacitor cells balancing in phase-shifted PWM-based cascaded H-bridge STATCOM," *IEEE Trans. Power Electron.*, vol. 32, no. 1, pp. 815–824, Jan. 2017.
[15] S. K. Kim, D. K. Choi, K. B. Lee, and Y. I. Lee, "Offset-free model predictive control for the power control of three-phase AC/DC converters," *IEEE Trans. Ind. Electron.*, vol. 62, no. 11, pp. 7114–7126, Nov. 2015.
[16] V. Blahnk, J. k, and Z. Peroutka, "Control of single-phase AC/DC converter with compensation of low-frequency disturbances," in *Proc. Int. Conf. Appl. Electron.*, Sep. 2011, pp. 1–4.
[17] A. Kuperman, "Proportional-resonant current controllers design based on desired transient performance," *IEEE Trans. Power Electron.*, vol. 30, no. 10, pp. 5341–5345, Oct. 2015.
[18] W. L. Chen and J. S. Lin, "One-dimensional optimization for proportional resonant controller design against the change in source impedance and solar irradiation in PV systems," *IEEE Trans. Ind. Electron.*, vol. 61, no. 4, pp. 1845–1854, Apr. 2014.
[19] A. Roshan, R. Burgos, A. C. Baisden, F. Wang, and D. Boroyevich, "A D-Q frame controller for a full-bridge single phase inverter used in small distributed power generation systems," in *Proc. 22nd Annu. IEEE Appl. Power Electron. Conf. Expo.*, Feb. 2007, pp. 641–647.
[20] R. Zhang, M. Cardinal, P. Szczesny, and M. Dame, "A grid simulator with control of single-phase power converters in D-Q rotating frame," in *Proc. IEEE 33rd Annu. IEEE Power Electron. Spec. Conf. Proc.*, 2002, vol. 3, pp. 1431–1436.
[21] M. Ciobotaru, R. Teodorescu, and F. Blaabjerg, "A new single-phase PLL structure based on second order generalized integrator," in *Proc. 37th IEEE Power Electron. Spec. Conf.*, Jun. 2006, pp. 1–6.
[22] A. Kulkarni and V. John, "A novel design method for SOGI-PLL for minimum settling time and low unit vector distortion," in *Proc. 39th Annu. Conf. IEEE Ind. Electron. Soc.*, Nov. 2013, pp. 274–279.
[23] P. Karamanakos, K. Pavlou, and S. Manias, "An enumeration-based model predictive control strategy for the cascaded H-bridge multilevel rectifier," *IEEE Trans. Ind. Electron.*, vol. 61, no. 7, pp. 3480–3489, Jul. 2014.
[24] M. Pastor and J. Durik, "Predictive control of grid-connected multilevel inverter with output LCL filter," *Elektronika ir Elektrotechnika*, vol. 21, no. 3, pp. 10–15, 2015.
[25] A. Dell'Aquila, M. Liserre, V. G. Monopoli, and P. Rotondo, "An energy-based control for an n-H-bridges multilevel active rectifier," *IEEE Trans. Ind. Electron.*, vol. 52, no. 3, pp. 670–678, Jun. 2005.
[26] H. Iman-Eini, J. L. Schanen, S. Farhangi, and J. Roudet, "A modular strategy for control and voltage balancing of cascaded H-bridge rectifiers," *IEEE Trans. Power Electron.*, vol. 23, no. 5, pp. 2428–2442, Sep. 2008.
[27] M. Pastor and J. Durik, "Comparison of MPC and PI controller for grid-connected cascade inverter," *Elektronika ir Elektrotechnika*, vol. 20, no. 6, pp. 46–50, 2014.
[28] Y. Yu, G. Konstantinou, B. Hredzak, and V. G. Agelidis, "Operation of cascaded H-bridge multilevel converters for large-scale photovoltaic power plants under bridge failures," *IEEE Trans. Ind. Electron.*, vol. 62, no. 11, pp. 7228–7236, Nov. 2015.
[29] A. Ghazanfari, H. Mokhtari, and M. Firouzi, "Simple voltage balancing approach for CHB multilevel inverter considering low harmonic content based on a hybrid optimal modulation strategy," *IEEE Trans. Power Del.*, vol. 27, no. 4, pp. 2150–2158, Oct. 2012.
[30] S. Gao and M. Barnes, "Phase-locked loop for AC systems: Analyses and comparisons," in *Proc. 6th IET Int. Conf. Power Electron., Mach. Drives*, Mar. 2012, pp. 1–6.
[31] D. Jank, J. Talla, T. Komrska, and Z. Peroutka, "Optimalization of SOGI PLL for single-phase converter control systems: Second order generalized integrator (SOGI)," in *Proc. Int. Conf. Appl. Electron.*, Sep. 2013, pp. 1–4.
[32] V. Blahnik, Z. Peroutka, and J. Talla, "Advanced control strategy for single-phase voltage source active rectifier with low harmonic emission," *J. Elect. Eng.—Elektrotechnicky casopis*, vol. 65, no. 2, pp. 121–124, 2014.
[33] D. N. Zmood and D. G. Holmes, "Stationary frame current regulation of PWM inverters with zero steady-state error," *IEEE Trans. Power Electron.*, vol. 18, no. 3, pp. 814–822, May 2003.
[34] R. Costa-Castello, R. Grino, and E. Fossas, "Resonant control of a single-phase full-bridge unity power factor boost rectifier," in *Proc. IEEE Int. Conf. Control Appl.*, Oct. 2007, pp. 599–604.
[35] T. Kosan, M. Jara, V. Blahnik, and Z. Peroutka, "A universal configurable sinusoidal modulator for H-bridge based converters implemented in FPGA," in *Proc. Int. Conf. Appl. Electron.*, Sep. 2015, pp. 111–114.
[36] T. Kosan, M. Jara, D. Janik, and Z. Peroutka, "Complete development platform for multi-level converters and complex control algorithms," in *Proc. 16th Int. Conf. Mechatronics*, Dec. 2014, pp. 152–157.
[37] *IEEE Recommended Practice and Requirements for Harmonic Control in Electric Power Systems*, IEEE Standard 519-2014 (Revision of IEEE Standard 519-1992), Jun. 2014, p. 1–29.
[38] D. G. Holmes and T. A. Lipo, *Pulse Width Modulation for Power Converters: Principles and Practice*, vol. 18. New York, NY, USA: Wiley, 2003.

Vojtech Blahnik (M'15) received the M.S. and Ph.D. degrees in electrical engineering from the University of West Bohemia (UWB), Pilsen, Czech Republic, in 2006 and 2011, respectively.

Since October 2010, he has been an R&D Engineer with the Regional Innovation Centre for Electrical Engineering, UWB. His main research interests include control of traction power converters and grid-connected converters.

Tomas Kosan received the M.S. and Ph.D. degrees in electrical engineering from the University of West Bohemia (UWB), Pilsen, Czech Republic, in 2008 and 2015, respectively.

Since 2011, he has been an R&D Engineer with the Regional Innovation Centre for Electrical Engineering, UWB. His main research interests include control and simulation of drives of modern transport systems and vehicles, and power electronics converters for medium-voltage applications with usage of field-gate-programmable arrays and modern multi-core microprocessors.

Zdeněk Peroutka (S'01–M'04) received the master's and Ph.D. degrees in electrical engineering from the University of West Bohemia (UWB), Pilsen, Czech Republic, in 2000 and 2004, respectively.

He is a Full Professor of power electronics and control systems and Vice-Dean for Science and Strategy with the Faculty of Electrical Engineering, UWB. From 2010 to 2016, he was a Scientific Director and Principal Investigator of the Regional Innovation Centre for Electrical Engineering (RICE), UWB. Since 2016, he has been the CEO and Principal Investigator of RICE. He authored or coauthored more than 150 papers in international journals and conferences. He is an inventor of two international patents. His main research interests include control of drives of modern transport systems and vehicles and power electronics converters for medium-voltage applications.

Jakub Talla received the M.S. and Ph.D. degrees in electrical engineering from the University of West Bohemia (UWB), Pilsen, Czech Republic, in 2006 and 2013, respectively.

Since October 2010, he has been an R&D Engineer with the Regional Innovation Centre for Electrical Engineering, UWB. His main research interests include control of ac drives and grid-connected converters, predictive control, and power management methods.